Original Research Article

In silico Binding and Interactions of Known Antivirals to the Dimer Pocket of the SARS-CoV-2 Main Protease

Nur Aqasyah Amran[1], Nur Alya Amirah Azhar[1], Nur Syahirunelisa Mohd Zubri[1], Nur Hannani Ahmad Rozani[2], Nurul Atikah Mohd Asri[3], Zafirah Liyana Abdullah[1], Fatahiya Mohamed Tap[2] and Siti Azma Jusoh[1]*

[1]Department of Pharmacology and Life Sciences, Faculty of Pharmacy, Universiti Teknologi MARA, Kampus Puncak Alam, 42300 Bandar Puncak Alam, Selangor, Malaysia
[2]School of Chemical Engineering, College of Engineering, Universiti Teknologi MARA, Kampus Bukit Besi, 23200 Dungun, Terengganu, Malaysia
[3]Faculty of Engineering Technology, Universiti Tun Hussein Onn Malaysia, 84600 Panchor, Johor, Malaysia

ABSTRACT

The devastating COVID-19 pandemic began in December 2019, catalyzed by the emergence of the SARS-CoV-2 beta-coronavirus strain. This inflicted global havoc, infecting over 767 million individuals and claiming more than 6.9 million lives by the end of 2023. Despite accelerated vaccine approvals significantly curbing infection rates and fatalities, the persistent spread of COVID-19 cases has been driven by evolving SARS-CoV-2 variants. The risk of future pandemics due to viral mutations emphasizes the urgent need for more effective antiviral drugs to prevent resistance. In this study, we explored the potential binding of small molecules to the dimer site of SARS-CoV-2 main protease (M^{pro}). We used the DogSiteScore program to predict the druggable sites, and Autodock Vina to evaluate the binding affinities of known antivirals. The results revealed that most of the antivirals exhibit higher binding affinities to the dimer site compared to the catalytic site. Notably, indinavir, nelfinavir, lopinavir, grazoprevir, and dolutegravir are among the top binders, surpassing -10 kcal/mol in the dimer site. Meanwhile, these antivirals exhibited affinities to the catalytic site that did not exceed -8.7 kcal/mol. These findings highlight the promising potential of the dimer site as an alternative target for developing specific COVID-19 inhibitors.

Keywords: Coronavirus; SARS-CoV-2; main protease; molecular docking

Corresponding author
Siti Azma Jusoh, PhD
Department of Pharmacology and Life Sciences,
Faculty of Pharmacy, Universiti Teknologi MARA,
Kampus Puncak Alam,
42300 Bandar Puncak Alam,
Selangor, Malaysia.
Email: sitiazma@uitm.edu.my

Received: 09 June 2024; accepted: 08 Aug 2024
Available online: 30 Aug 2024
http://doi.org/10.24191/IJPNaCS.v7i2.05

1.0 Introduction

Coronaviruses are responsible for severe acute respiratory syndrome coronavirus (SARS-CoV) and Middle East respiratory syndrome coronavirus (MERS-CoV), affecting both humans and animals (1). The virus behind the COVID-19 outbreak, SARS-CoV-2, shares sequence and structural similarities with other coronaviruses such as MERS-CoV and SARS-CoV (2). These similarities are fundamental in understanding the disease and investigating potential treatments. Throughout the COVID-19 pandemic, SARS-CoV-2 has mutated to numerous variants, including notable strains like Alpha, Beta, Gamma, Delta and Omicron (3). The emergence of new coronavirus variants poses threats to the effectiveness of the current vaccines and risks of future pandemics.

SARS-CoV-2 belongs to the family of beta-coronaviruses, which are envelope viruses consisting of a single-stranded positive-sense RNA genome with approximately 30,000 nucleotides (4). The viral open-reading frames translate into two overlapping polyproteins, namely pp1a and pp1ab. When internalized within host cells, these polyproteins undergo cleavage processes, producing individual proteins essential for viral replication and transcription (5,6). The polyproteins encode four structural and 16 non-structural proteins. The structural proteins include nucleocapsid, spike, membrane protein, and envelope (7). One of the non-structural proteins is the main protease (M^{pro}), also known as 3-chymotrypsin-like cysteine protease (3CLpro) (8). M^{pro} is responsible for the 11 cleavage sites of the polyprotein (9). Due to its crucial role, M^{pro} has become the primary target for most drug development efforts aimed at inhibiting SARS-CoV-2 (10-12). In addition, M^{pro} is highly conserved among coronaviruses and cleaves polypeptides immediately after the glutamine residue, which differs from human proteases. Consequently, inhibitors targeting M^{pro} are likely to be highly selective and unlikely to be toxic to humans (13-15).

The functional structure of SARS-CoV-2 M^{pro} is characterized by a homodimeric arrangement, where two perpendicular monomers intertwine (13). Each monomer consists of three distinct domains: I, II, and III. Domains I (residues 10–99) and II (residues 100–182) exhibit a structure similar to that of chymotrypsin, featuring a unique six-stranded antiparallel β-barrel fold. The connection between domains II and III is facilitated by a flexible loop (residues 183–198), which can dynamically adopt either an elongated or condensed helical configuration (16). The active site of M^{pro} lies within the cleft between domains I and II, accommodating the catalytic dyad residues, HIS41 and CYS145. These residues play a crucial role in proteolytic cleavage (17). Domain III, located at the C-terminal region (residues 198–303), plays a pivotal role in facilitating dimerization through an intermolecular salt-bridge interaction between Glu290 and Arg4 (18). Dimerization brings the active sites of the two monomers into close proximity, allowing efficient substrate binding and catalysis (13). This ensures that both monomers adopt the proper conformation required for catalytic function, facilitated by interactions between N-fingers from each protomer at Glu166, shaping the substrate-binding site's S1 pocket (13).

There are more than hundreds of X-ray crystallographic structures of M^{pro} bound to small-molecule compounds in the catalytic site, representing most of the studies focusing on the orthosteric pocket. A study by Jin et al. in 2020 (19) suggested significant inhibition and the formation of a stable covalent bond between the N3 inhibitor and the active site of M^{pro}. Since the catalytic site of SAR-CoV-2 M^{pro}

shares 100% sequence similarity with the M^{pro} of SARS-CoV (20), drugs designed to inhibit the function of SARS-CoV-2 M^{pro} may also interact with other coronaviruses. The findings indicate that binding to the catalytic site of M^{pro} leads to inhibition of SARS-CoV-2 (21). The catalytic dyad residues, HIS41 and CYS145, are capable of forming covalent bonds with potential COVID-19 inhibitors such as peptidomimetics (N3), α-ketoamides, and vinylsulfones (19, 14, 20). While many known covalent drugs are potent, there are also concerns that covalent interactions may form irreversible bonds, potentially leading to unintended consequences such as off-target effects or interference with biological processes, which could cause adverse effects and toxicity (14).

The catalytic site of M^{pro} is an orthosteric pocket, which shares highly similar residues and pocket structure with other coronaviruses. Consequently, the development of COVID-19 inhibitors primarily targets the catalytic pocket of M^{pro}, aiming to inhibit various types of coronaviruses (19, 22, 23). However, the high similarity in binding sites may reduce drug effectiveness and lead to adverse effects due to nonspecific binding (24). In modern drug discovery, a rational design approach explores allosteric drugs to create more precise, selective, and safer medications compared to those targeting orthosteric sites (25). Allosteric drugs bind to other pockets on the receptor, capable of altering the active site conformation and reducing substrate binding, thereby inhibiting proper receptor function. A study using Gaussian accelerated molecular dynamics (MD) simulations (GaMD) of the M^{pro} dimer revealed the locations of cryptic and potential allosteric pockets, predicted to be highly druggable (2). In line with computational studies, X-ray crystallography and other structural determination methods have also reported the binding of small molecules to different cavities on M^{pro} other than the catalytic site (26, 27). Alzyoud et al. (24) reviewed six experimental pockets of M^{pro} bound to small molecules, representing additional pocket cavities apart from the catalytic site. Among these, two X-ray structures (5RGQ and 5RFA) of M^{pro} exhibited the same pocket location on the surface of one of the protomers, representing a deep groove between the catalytic domain (domain I and domain II) and the dimerization domain (domain III) (Supplementary Fig. 1) (26, 27). Interestingly, this surface pocket has a small opening connecting to the internal cavity of M^{pro}, allowing the bound ligand to interact with residues in the dimer interface. Another X-ray structure of M^{pro} (7AGA) also reported ligand binding at the same allosteric region; however, this pocket lacks a visible opening to the internal cavity of the Mpro dimer pocket interface. The dynamics of this pocket may involve transient openings, facilitating ligand access and binding. Overall, this suggests a flexible and adaptable nature that can be exploited for therapeutic interventions.

Moreover, in identifying the effectiveness of therapeutics effects on SARS-CoV-2, the repurposing of known antivirals has gained intention. Repurposing existing drugs with known safety profiles and mechanisms of action may reveal new targets and offer a potential shortcut to accelerate the development of effective treatments (28). For example, zidovudine, originally designated for cancer treatment, was repurposed to combat HIV/AIDS (28). This transformation was accomplished through an innovative *in vitro* screening approach and marked a significant milestone as the first FDA-approved anti-HIV drug. Several drugs including remdesivir and favipiravir targeting RNA-

dependent RNA polymerase (RdRp), along with lopinavir-ritonavir and darunavir targeting the protease, are currently under investigation for their ability to hinder the replication of SARS-CoV-2 and alleviate symptoms of COVID-19 (29-32).

This study focuses on a dimer pocket of M^{pro} to investigate the binding of known antivirals and explore it as a potential new binding site. Using the molecular docking method, the dimer pocket was screened with 15 known antiviral compounds. The resulting binding affinities from this docking process were then compared to those of the M^{pro} active site, aiming to identify alternative therapeutic targets and enhance the understanding of antiviral interactions.

2.0 Materials and Methods

2.1 Protein and Ligand Structure Preparation

The crystal structures of the SARS-CoV-2 M^{pro} represented by PDB ID 6LU7, 7NT3, and 7EIN were obtained from the Protein Data Bank (PDB) (https://www.rcsb.org/). Among these structures, 6LU7 (19), which consists of a monomer unit, was utilized for the docking reference at the catalytic site. Both 7NT3 and 7EIN are dimers and were utilized in this work for the docking into the dimer pocket located between two monomer units (22,23). In addition to the crystal structures, we also utilized a snapshot of SARS-CoV-2 M^{pro} from a one microsecond trajectory of Gaussian-accelerated molecular dynamics (GaMD) obtained from the study of Sztain et al. (2021) (2). This snapshot, named MD-272, represents the conformational dynamics of M^{pro} and was selected based on the largest cavity within its dimer pocket. Subsequently, we optimized the protein structures using PDB2PQR (33) based on the CHARMM force field (34) and employed PROPKA (35) to protonate the proteins at pH 7.0. Finally, the resulting files in PQR format were converted to PDB format using Open Babel (36). For the ligands, structural information of 15 known antivirals (Fig. 1) was retrieved from the PubChem database (https://pubchem.ncbi.nlm.nih.gov/). Open Babel was employed to convert the SDF format to the PDB format, while simultaneously protonating the ligands at pH 7.0.

Prior to the molecular docking steps, both the proteins and ligands were prepared using AutoDock Tools (ADT) (37). The preparatory steps included eliminating water, solvent molecules and other bound ligands. Additionally, Kollman charges, hydrogen atoms were added. Finally, ADT generated the output structures of proteins and ligands in PDBQT format, ready as input files for molecular docking.

2.2 Binding Pocket Prediction

DogSiteScorer (38) (https://proteins plus.zbh.uni-hamburg.de/#dogsite) was utilized to predict the druggable binding pockets for the SARS-CoV-2 M^{pro}. The method utilizes an algorithm that analyzes surface properties, hydrophobicity, shape, and volume of cavities or crevices on the protein surface, allowing for the detection of druggable binding pockets. The 3D structure of the protein in PDB format was used as the input. Upon execution with default setting parameters, the method generated druggability scores for each predicted pocket along with other pocket information. For this study, we selected the predicted druggable pockets with scores ≥ 0.7 for further analysis (Fig. 2).

2.3 Molecular Docking

Autodock Vina was employed as the docking program (39). 15 studied antivirals (Fig. 1) were docked to the M^{pro}'s catalytic site and the dimer pocket.

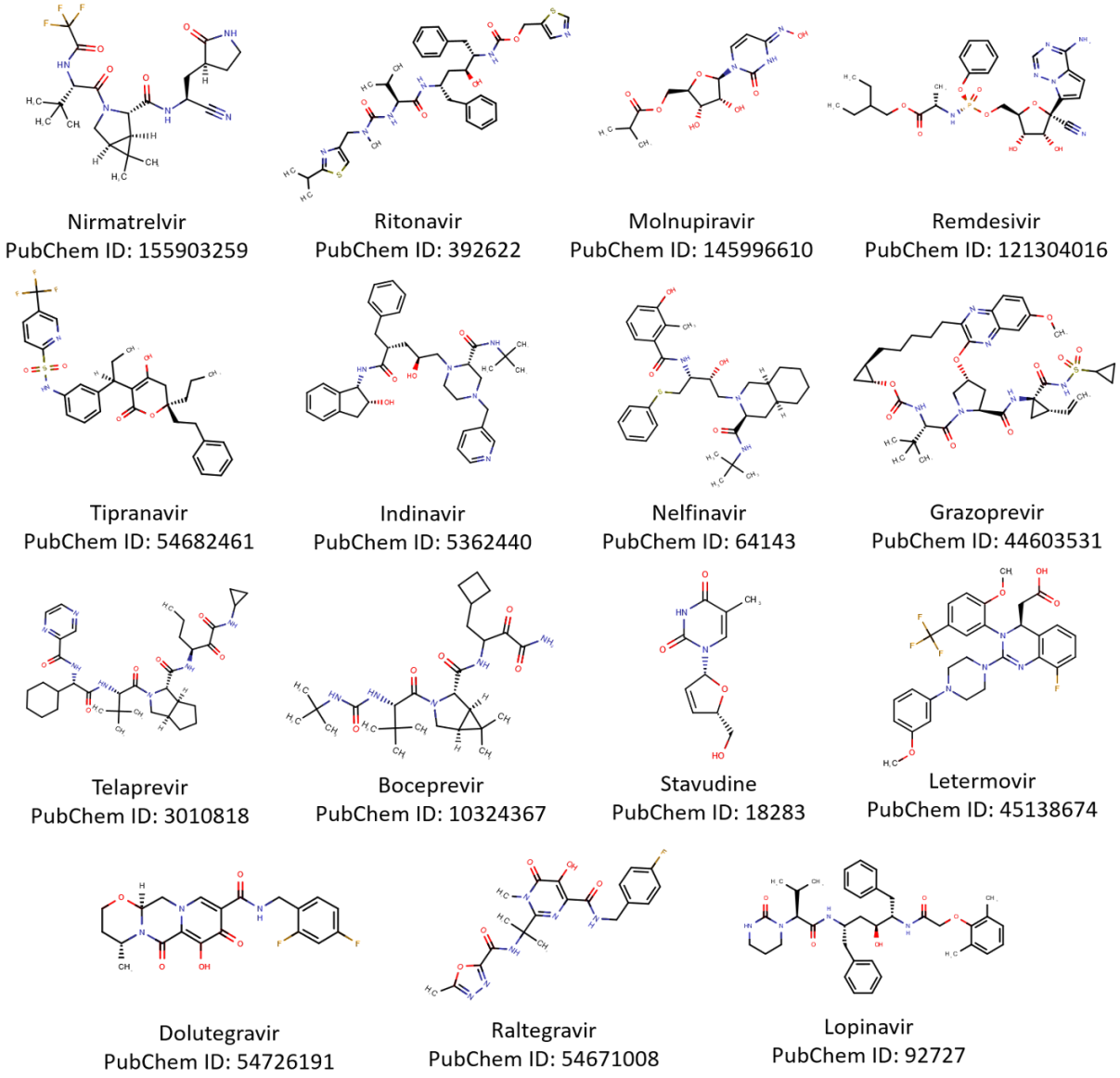

Fig. 1: 2D structures of the 15 known antiviral drugs used for the molecular docking study of the SARS-CoV-2 M^{pro}

The grid center coordinates were set at X = -13.0, Y = 15.9, Z = 68.2 for 6LU7, X = -2.9, Y = 2.1, Z = -19.6 for 7NT3, X = 6.2, Y = -10.4, Z = 28.2 for 7EIN and X = 52.8, Y = 46.6, Z = 49.2 for MD-272. The grid dimensions of the box size were either 30 x 30 x 30 or 40 x 40 x 40 for the dimer pocket, while for the catalytic pocket, it was set to 28 x 28 x 28. The exhaustiveness was set to 20 for all docking runs. Each compound underwent triplicate docking runs, and the best poses were selected based on correct binding pocket placement, structural orientations, and binding affinity values. The binding affinity values presented in the results section represent the average of the triplicates. Biovia Discovery Studio Visualizer (40) was utilized to visualize

the docked poses and generate 2D interaction plots.

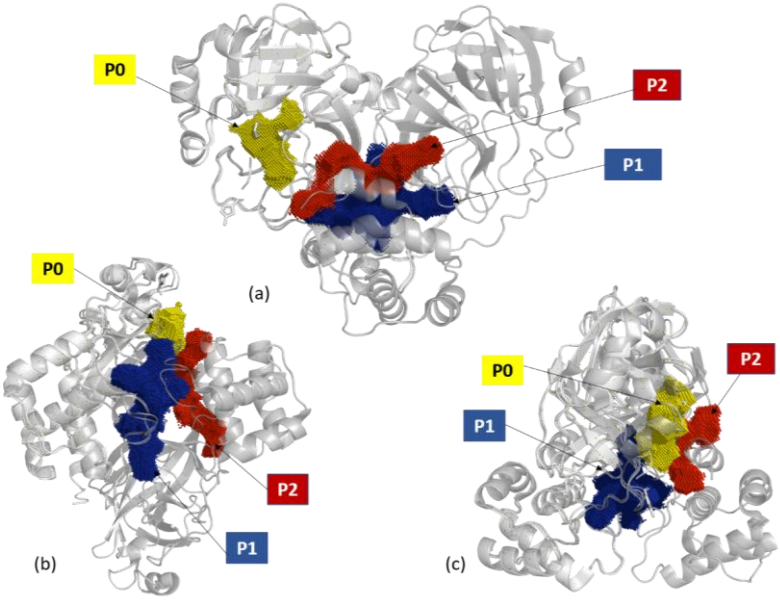

Fig. 2: Druggable pocket predictions using DogSiteScorer for the SARS-CoV2 M^{pro}. The protein is represented as a cartoon. The P0, P1 and P2 blobs represent the catalytic pocket, the dimer pocket and the surface-pocket, respectively. The visualization is viewed from front (a), bottom (b), and side (c) of the SARS-CoV2 M^{pro}.

3.0 Results

3.1 Prediction of Druggable Pockets

DogSiteScorer was utilized in this study to predict drug binding sites of M^{pro}. The program identified at least three druggable pockets, scoring between 0.14 and 0.82 (Supplementary Table 5). A higher score indicates greater drug affinity for the pocket. In our study, we focused on the top three druggable pockets with scores exceeding 0.7 (Fig. 2 & Supplementary Table 6). One of the top pockets was the catalytic pocket of M^{pro}, namely P0 that obtained the druggable score of 0.64 (Supplementary Table 6). The dimer pocket, which is the pocket that formed between the two protomers, namely P1 exhibited higher druggable score than the catalytic pocket (0.80-0.81). This pocket presented the largest cavity (1043.89 $Å^3$ - 2732.44 $Å^3$) and large surface area (1314.21 $Å^2$ - 3396.64 $Å^2$). It was also worth noting that the hydrophobicity of the dimer pocket was also higher than the catalytic pocket.

Additionally, DogSiteScorer identified a smaller pocket, namely P2 located on the surface of M^{pro} adjacent to the catalytic pocket. This pocket had a higher druggable score than the catalytic pocket (0.82). P2 exists on both sides of the Mpro protomer, with a volume of up to 671.2 $Å^3$. However, in this study, only the dimer pocket was selected for further analysis using the molecular docking method.

3.2 Docking to the Dimer Pocket

Docking of the 15 known antivirals was performed on both the dimer pocket and the catalytic site of M^{pro}. Overall, most of the compounds exhibited higher affinities when binding to the dimer pocket compared to the catalytic site of M^{pro}. The highest binding affinity represent the antivirals that docked to the catalytic site

was -8.7 kcal/mol. In contrast, indinavir demonstrated a binding affinity exceeding -10.0 kcal/mol for the dimer pocket across all the three protein structures, while 14 other antiviral compounds displayed binding affinities ranging from -7.3 to -10.2 kcal/mol. In both binding pockets, the lowest binding affinity was represented by stavudine (~ -6.0 kcal/mol). The docking results of the dimer pocket in both x-ray structures of M^{pro} (PDB ID 7NT3 and 7EIN) were similar. It is worth noting that another structure of M^{pro} used for this docking study, namely MD-272 resulted in five compounds that exhibited binding affinities of -10.0 kcal/mol and higher (indinavir, nelfinavir, grazoprevir, dolutegravir, lopinavir). This M^{pro} structure was a snapshot obtained from the one microsecond trajectory of GaMD simulations from the study of Sztain et al. (2021) (2) that was selected based on its largest volume of the dimer pocket. These results highlight that a larger binding pocket may enhance higher binding affinities, that could be explained based on flexibility of the compounds to optimize the conformation in the pocket cavity. Visualization of the docking results and binding affinities to the dimer pocket are shown in Fig. 3 and Table 1, respectively. Additional binding affinity results of the replicates for each protein structure are shown in Supplementary Table 1 - 4.

3.3 Interactions of the Antivirals in the Dimer Pocket of M^{pro}

Further analysis was conducted to the docked antiviral compounds with the top highest binding affinities to the dimer pocket of M^{pro}. Three antivirals were selected, which were indinavir, grazoprevir and lopinavir. For each antiviral, inter-atomic interactions between the protein residues and the compound were analyzed. In addition, three different docked poses are presented in order to illustrate possible binding modes between M^{pro} and the studied antivirals that may occur in the dimer pocket. Detailed information including type of interactions, amino acids involved, and distances of the interactions formed between the selected antivirals and SARS-CoV-2 M^{pro} for the top three poses are shown in Supplementary Table 7.

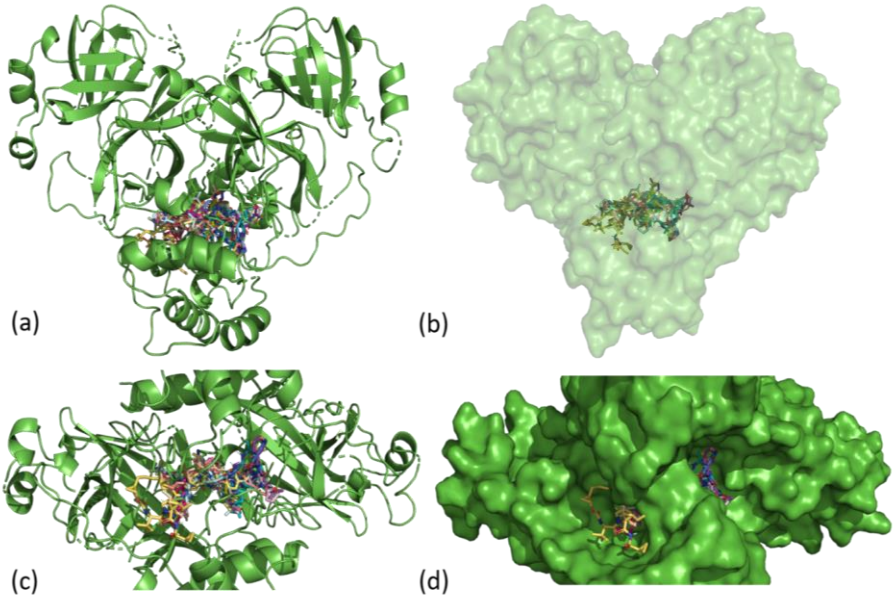

Fig. 3: Docking of 15 known antiviral drugs to the dimer pocket of SARS-CoV-2 M^{pro}. Front view (a, b) and bottom view (c, d). The cartoon and solid surface represent the M^{pro} and the stick represents the antiviral molecules

Table 1: Binding affinities of 15 known antivirals to the catalytic site of the SARS-CoV-2 M^{pro} (PDB ID 6LU7) and the dimer interface pocket (PDB ID 7NT3, PDB ID 7EIN and MD-272)

No	Antivirals	Binding Affinities (kcal/mol)			
		6LU7	7NT3	7EIN	MD-272
		Catalytic Site		Dimer Pocket	
1	Nirmatrelvir	-8.6	-8.8	-8.4	-9.7
2	Ritonavir	-7.5	-9.4	-9.2	-9.6
3	Molnupiravir	-7.0	-7.3	-8.0	-7.5
4	Remdesivir	-7.9	-8.7	-8.4	-9.4
5	Tipranavir	-7.6	-8.7	-9.8	-9.9
6	Indinavir	-8.0	-10.0	-10.0	-10.2
7	Nelfinavir	-8.3	-9.1	-9.4	-10.0
8	Grazoprevir	-8.1	-9.2	-9.9	-10.1
9	Telaprevir	-7.3	-9.8	-9.3	-9.5
10	Boceprevir	-7.2	-9.0	-8.7	-8.8
11	Stavudine	-6.2	-6.1	-6.3	-6.6
12	Letermovir	-7.4	-9.6	-8.6	-8.7
13	Dolutegravir	-8.7	-9.0	-9.3	-10.0
14	Raltegravir	-8.7	-9.6	-9.1	-9.9
15	Lopinavir	-8.0	-9.0	-9.6	-10.2

3.3.1 Interactions with Indinavir

The docking of indinavir was performed on all three M^{pro} structures, resulting in binding affinities of approximately -10.0 kcal/mol (Table 1). Fig. 4 illustrates a detailed depiction of the interactions between the dimer pocket of M^{pro} and indinavir, showcasing the top three poses derived from the docking results. In each of these docked poses, indinavir maintains the same conformation and orientation, interacting with three residues from both chain A and B: ARG4-A, GLU288-B, and ARG4-B. Among these residues, GLU288-B forms five types of interactions, including three conventional hydrogen bonds, one carbon hydrogen bond, and one pi-anion bond. ARG4-B participated in four interactions, comprising two pi-alkyl, one alkyl, and one pi-cation interaction. Additionally, LYS5-B exhibited four interactions, involving two pi-donor hydrogen bonds and two alkyl interactions. Notably, the remaining interacting residues, which encompassed ARG4-A, LEU282-A, ARG131-B, GLY283-A, LYS5-A, LYS137-B, LYS137-A, LEU286-A, GLU288-A, and GLU290-A interacted with indinavir fewer than four times in all poses.

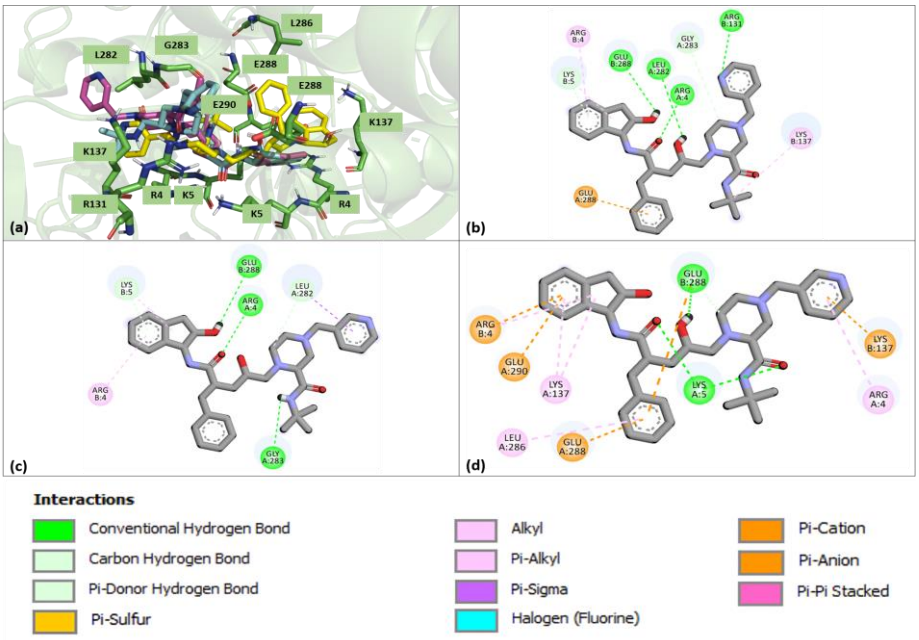

Fig. 4: Interactions between indinavir and M^{pro} in the dimer pocket. (a) Superimposition of the 3 top poses of indinavir docked to M^{pro}. Residues interacting with indinavir are shown Pose 1 (b) Pose 2 (c), and Pose 3 (d).

3.3.2 Interactions with Grazoprevir

Grazoprevir was one of the top five antivirals that exhibited high binding affinities to the M^{pro} dimer pocket (-9.1 to -10.1 kcal/mol) (Table 1). Fig. 5 illustrates the intermolecular interactions between grazoprevir and the dimer pocket. Grazoprevir interacts twice with six residues: LYS137-A (conventional hydrogen bond, alkyl), LEU286-A (alkyl), LYS5-B (conventional hydrogen bond, alkyl), ASN214-B (carbon hydrogen bond), SER284-B (carbon and conventional hydrogen bond), and PHE291-B (pi-sulfur, pi-alkyl). On the other hand, THR199-A, GLU288-A, ALA285-B, LYS5-A, TYR239-A, GLY283-B, and LEU282-B interact only once with this antiviral. In total, 13 residues are involved in 19 interactions with grazoprevir.

3.3.3 Interactions with Lopinavir

Lopinavir exhibited binding affinities between -9.0 to -10.2 kcal/mol to the M^{pro} dimer pocket (Table 1). The potential interactions in the dimer pocket are shown in three top docking poses (depicted in Fig. 6). The three top poses display different structural orientation and confirmation of the compound. In all three poses, both LYS5-A and LYS5-B form interactions with lopinavir. Compared to LYS5-B, LYS5-A engaged in a higher number of interactions, including three hydrogen bonds and two pi-alkyl interactions. Furthermore, lopinavir might also remain stable in the dimer pocket through other interactions, such as two conventional and one carbon hydrogen bond with GLY283-A. In addition, LYS5-B participates in three interactions, comprising one conventional hydrogen bond and two pi-alkyl interactions. Another residue, ARG4-B forms two pi-cation and one alkyl interactions. Other residues, SER284-A, SER284-B, LYS137-B, LEU286-B, ARG4-A, GLU288-A, LYS137-A and GLU288-B exhibited fewer than three interactions with lopinavir. Overall, a total of 12 residues contributed to the 25 interactions observed with lopinavir in the dimer pocket.

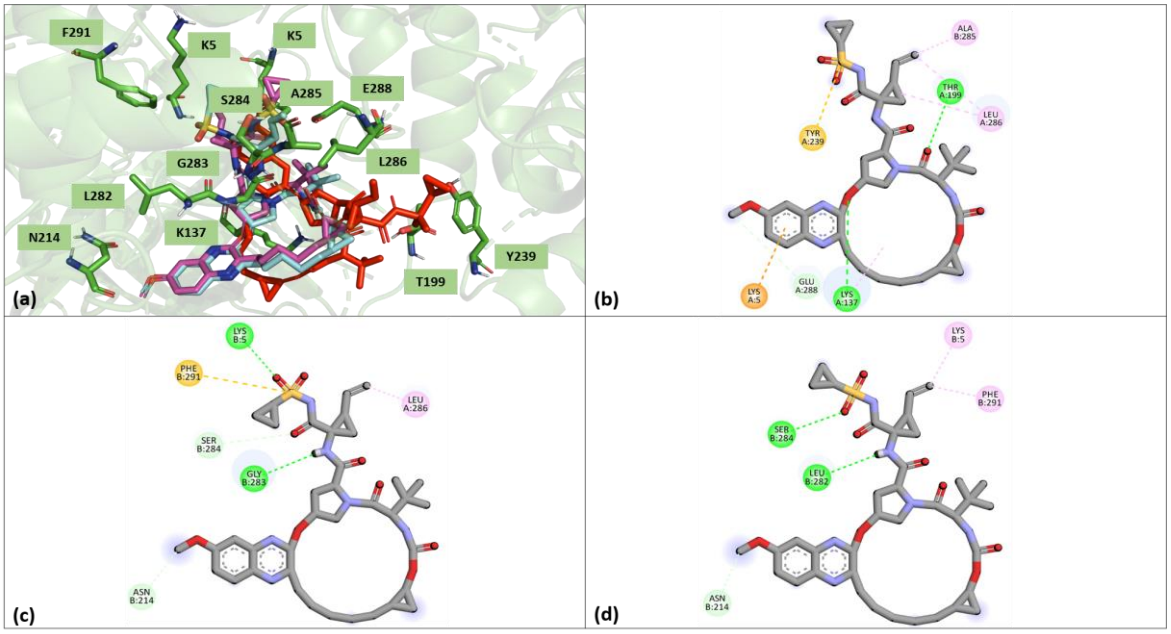

Fig. 5: Interactions between grazoprevir and M^{pro} in the dimer pocket (refer legends in Fig. 4). (a) Superimposition of the 3 top poses of grazoprevir docked to the M^{pro} dimer pocket. Residues interacting with grazoprevir are shown in Pose 1 (b) Pose 2 (c), and Pose 3 (d).

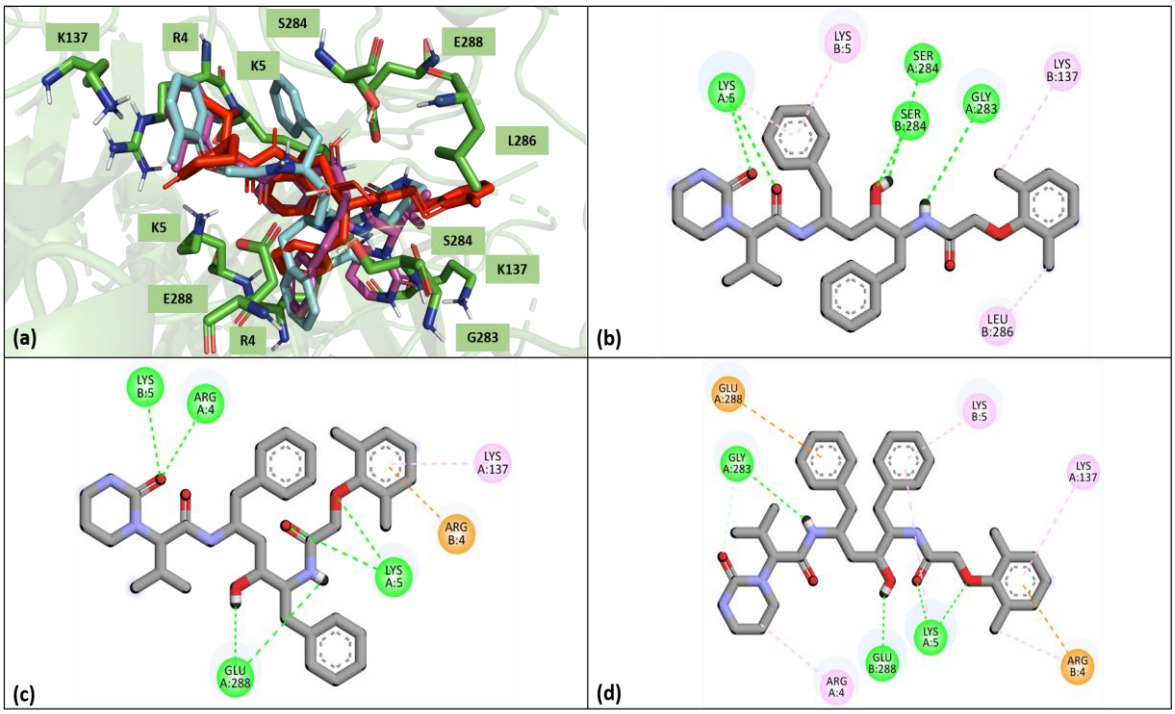

Fig. 6: Interactions between lopinavir and M^{pro} in the dimer pocket. (refer legends in Fig. 4). (a) Superimposition of the 3 top poses of lopinavir docked to the M^{pro} dimer pocket. Residues interacting with lopinavir in Pose 1 (b) Pose 2 (c), and Pose 3 (d).

4.0 Discussion

The global health crisis initiated by the SARS-CoV-2 strain of coronavirus has presented significant challenges worldwide, particularly due to the emergence of mutations that compromise the efficacy of the existing treatments. This underscores the urgent need for the development of novel antiviral medications that can effectively target key viral proteins. One such protein, M^{pro}, is crucial for processing viral polyproteins in coronaviruses. Its high structural and sequence conservation across different coronavirus strains makes M^{pro} an ideal target for broad-spectrum antiviral therapy development (Supplementary Fig. 2). In this study, we focused on the dimer pocket of M^{pro} as a potential binding site implementing the rational drug design strategy targeting SARs-CoV-2.

The initial finding based on the DogSiteScorer program, indicates that the dimer pocket of M^{pro} possesses a higher druggable score compared to the catalytic pocket. This higher score suggests that the dimer pocket offers significant advantages for drug targeting. One key advantage is the greater specificity and selectivity due to the lower similarity of residues within the dimer pocket, which can help design more precise inhibitors for SARS-CoV-2. Furthermore, the larger volume of the dimer pocket allows for more flexibility in ligand binding. This flexibility can lead to stronger and more stable binding interactions, as ligands can adopt optimal conformations within the pocket. Supporting this, the MD snapshot obtained from Sztain et al. (2021) (2) revealed that M^{pro} structures with the largest dimer pocket volumes exhibited the highest binding affinities for most docked antivirals. This correlation between larger pocket volumes and higher druggability is well-documented (38), as larger pockets can accommodate a variety of ligands and facilitate more extensive interactions, including hydrogen bonds and hydrophobic interactions. Additionally, the higher number of hydrogen bond acceptors and donors in the dimer pocket compared to the orthosteric pocket further enhances its potential as a drug target. These features collectively make the dimer pocket a promising target for developing effective antiviral therapies against SARS-CoV-2 and potentially other coronaviruses.

Further docking analysis of 15 known antivirals showed higher binding affinities to the dimer pocket than the catalytic site of M^{pro}. All antivirals docked to the dimer pocket scored binding affinities between -8.4 to -10.2 kcal/mol except for molnupiravir and stavudine. Conversely, only 7 out of 15 of the antivirals scored binding affinities between -8.0 to 8.7 kcal/mol (nirmatrelvir, indinavir, nelfinavir, grazoprevir, dolutegravir, raltegravir and lopinavir) to the catalytic site. Similar results were reported by other docking studies targeting the catalytic pocket of M^{pro} (41-44). The top three antivirals docked to the catalytic site were dolutegravir and raltegravir, which are the integrase inhibitors targeting HIV, then followed by nirmatrelvir, the recently approved antiviral in combination with ritonavir, packaged as Paxlovid for the COVID-19 treatment. Paxlovid was clinically shown to reduce 89% risk of infected patients from progression to severe stage of COVID-19 (45). From the x-ray crystallographic structure, nirmatrevir was observed to form a covalent bond to CYS145, one of the catalytic dyad residues (46) of M^{pro}, which exhibited potent inhibition to the M^{pro} activity across a broad spectrum of coronaviruses (47). On the other hand, the top antivirals with the highest affinity for the dimer pocket were indinavir, lopinavir and grazoprevir (-9.0 to -10.2 kcal/mol). These are protease inhibitors designed to target HIV (indinavir, lopinavir) and HCV

(grazoprevir). The docked compounds adopted several different conformations and orientations in the dimer pocket, possibly due to its large volume cavity. Based on the docking analysis, the most amino acid residues that interacted with the antivirals located within the dimer pocket interface were ARG4-B, LYS5-A, LYS5-B, LYS137-A, GLY283-A and GLU288-B.

An *in silico* study by Liang et al. (48) described the dimer pocket of SARS-CoV-2 M^{pro} as a highly reactive binding site, based on consistent strong ligand preferences observed during blind docking analysis. Utilizing MD simulations, the same study identified that ritonavir binding in the dimer pocket exhibited hydrogen bonds with residues LYS5-A, PHE3-B, LYS5-B, TRP207-A, TRP207-B, GLY283-B, LEU286-A, and GLU288-B. These residues were also found to interact with the antivirals presented in our study, notably LYS5-A and LYS5-B (Supplementary Table 8). Additionally, their study employed molecular mechanics Poisson-Boltzmann surface area (MMPBSA) analysis, revealing stronger binding energy for ritonavir in the dimer pocket (24.4 kcal/mol) compared to the catalytic site (17.9 and 17.2 kcal/mol) (48). This highlights the potential of the dimer pocket as a promising target for drug binding, reinforcing the significance of our findings.

5.0 Conclusion

Our study underscores the dimer pocket of M^{pro} as a highly promising target for antiviral drug development against SARS-CoV-2. The dimer pocket's higher druggability score, larger volume, and greater specificity, compared to the catalytic pocket, suggest significant advantages for designing potent inhibitors. Our docking analysis demonstrated that known antivirals bind more strongly to the dimer pocket, indicating its potential for effective drug binding. Future computational studies could proceed with MD simulations and MM/PBSA analysis, which can provide insights into the dynamic behavior and stability of the protein-ligand complex and help predict the binding affinities of potential drug candidates. Experimental approaches such as X-ray crystallography, surface plasmon resonance (SPR), and cell-based assays are vital for confirming the binding interactions between M^{pro} and the ligand. Through these combined approaches, we hope to contribute to the ongoing efforts in developing new treatments targeting the dimer pocket of M^{pro}.

Author Contributions

NAA: performed most of the experiment, analysis, and wrote the original draft. **SAJ**: Project administration, conceptualization, supervision, and approval of the final draft. **NSMZ, NAMA, NAAA** and **NHAR**: performed some computational analysis. **ZLA** and **FMT**: Manuscript review and editing. All authors have read and agreed to the published version of the manuscript.

Acknowledgement

We acknowledge MAKERLAB UiTM and Faculty of Pharmacy, Universiti Teknologi MARA (UiTM) Cawangan Selangor, Malaysia for the computing facilities used for this project. This project was funded by the UiTM internal grant, DUCS: 600-UiTMSEL (PI. 5/4) (072/2022).

Conflicts of Interest

The authors declare no conflict of interest.

References

1. Wu D, Wu T, Liu Q, Yang Z. The SARS-CoV-2 outbreak: What we know. Int J Infect Dis. 2020;94:44–8.

2. Sztain T, Amaro R, McCammon JA. Elucidation of Cryptic and Allosteric Pockets within the SARS-CoV-2 Main Protease. J Chem Inf Model. 2021;61(7):3495–501.

3. Parums DV. Editorial: A Rapid Global Increase in COVID-19 is Due to the Emergence of the EG.5 (Eris) Subvariant of Omicron SARS-CoV-2. Med Sci Monit Int Med J Exp Clin Res. 2023;29:e942244-1-e942244-4.

4. Li X, Geng M, Peng Y, Meng L, Lu S. Molecular immune pathogenesis and diagnosis of COVID-19. J Pharm Anal. 2020;10(2):102–8.

5. Zhou P, Yang XL, Wang XG, Hu B, Zhang L, Zhang W, et al. A pneumonia outbreak associated with a new coronavirus of probable bat origin. Nature. 2020;579(7798):270–3.

6. Wu F, Zhao S, Yu B, Chen YM, Wang W, Song ZG, et al. A new coronavirus associated with human respiratory disease in China. Nature. 2020;579:265–9.

7. Satarker S, Nampoothiri M. Structural Proteins in Severe Acute Respiratory Syndrome Coronavirus-2. Arch Med Res. 2020;51(6):482–91.

8. Wu C, Liu Y, Yang Y, Zhang P, Zhong W, Wang Y, et al. Analysis of therapeutic targets for SARS-CoV-2 and discovery of potential drugs by computational methods. Acta Pharm Sin B. 2020;10(5):766–88.

9. Hilgenfeld R. From SARS to MERS: crystallographic studies on coronaviral proteases enable antiviral drug design. FEBS J. 2014;281(18):4085–96.

10. Das S, Sarmah S, Lyndem S, Singha Roy A. An investigation into the identification of potential inhibitors of SARS-CoV-2 main protease using molecular docking study. J Biomol Struct Dyn. 2021;39(9):3347–57.

11. Patel CN, Jani SP, Jaiswal DG, Kumar SP, Mangukia N, Parmar RM, et al. Identification of antiviral phytochemicals as a potential SARS-CoV-2 main protease (Mpro) inhibitor using docking and molecular dynamics simulations. Sci Rep. 2021;11(1):20295.

12. Gupta S, Singh AK, Kushwaha PP, Prajapati KS, Shuaib M, Senapati S, et al. Identification of potential natural inhibitors of SARS-CoV2 main protease by molecular docking and simulation studies. J Biomol Struct Dyn. 2021;39(12):4334–45.

13. Zhang L, Lin D, Sun X, Curth U, Drosten C, Sauerhering L, et al. Crystal structure of SARS-CoV-2 main protease provides a basis for design of improved α-ketoamide inhibitors. Science. 2020;368(6489):409–12.

14. Pillaiyar T, Manickam M, Namasivayam V, Hayashi Y, Jung SH. An Overview of Severe Acute Respiratory Syndrome–Coronavirus (SARS-CoV) 3CL Protease Inhibitors: Peptidomimetics and Small Molecule Chemotherapy. J Med Chem. 2016;59(14):6595–628.

15. Mengist HM, Dilnessa T, Jin T. Structural Basis of Potential Inhibitors Targeting SARS-CoV-2 Main Protease. Front Chem. 2021; 9:622898.

16. Arya R, Kumari S, Pandey B, Mistry H, Bihani SC, Das A, et al. Structural insights into SARS-CoV-2 proteins. J Mol Biol. 2021;433(2):166725.

17. Huang C, Wei P, Fan K, Liu Y, Lai L. 3C-like Proteinase from SARS Coronavirus Catalyzes Substrate Hydrolysis by a General Base Mechanism. Biochemistry. 2004;43(15):4568–74.

18. Shi J, Song J. The catalysis of the SARS 3C-like protease is under extensive regulation by its extra domain. FEBS J. 2006;273(5):1035–45.

19. Jin Z, Du X, Xu Y, Deng Y, Liu M, Zhao Y, et al. Structure of Mpro from SARS-CoV-2 and discovery of its inhibitors. Nature. 2020;582(7811):289–93.

20. Boike L, Henning NJ, Nomura DK. Advances in covalent drug discovery. Nat Rev Drug Discov. 2022;21(12):881–98.

21. Boras B, Jones R, Anson B, Arenson D, Aschenbrenner L, Bakowski M, et al. Discovery of a Novel Inhibitor of Coronavirus 3CL Protease as a Clinical Candidate for the Potential Treatment of COVID-19. BioRxiv Prepr Serv Biol. 2020-2029.

22. Sutanto F, Shaabani S, Oerlemans R, Eris D, Patil P, Hadian M, et al. Combining High-Throughput Synthesis and High-Throughput Protein Crystallography for Accelerated Hit Identification. Angew Chem Int Ed Engl. 2021;60(33):18231–9.

23. Fu L, Shao S, Feng Y, Ye F, Sun X, Wang Q, et al. Mechanism of Microbial Metabolite Leupeptin in the Treatment of COVID-19 by Traditional Chinese Medicine Herbs. Rappuoli R, editor. mBio. 2021;12(5):e02220-21.

24. Alzyoud L, Ghattas MA, Atatreh N. Allosteric Binding Sites of the SARS-CoV-2 Main Protease: Potential Targets for Broad-Spectrum Anti-Coronavirus Agents. Drug Des Devel Ther. 2022;16:2463–78.

25. Wagner JR, Lee CT, Durrant JD, Malmstrom RD, Feher VA, Amaro RE. Emerging Computational Methods for the Rational Discovery of Allosteric Drugs. Chem Rev. 2016;116(11):6370–90.

26. Günther S, Reinke PYA, Fernández-García Y, Lieske J, Lane TJ, Ginn HM, et al. X-ray screening identifies active site and allosteric inhibitors of SARS-CoV-2 main protease. Science. 2021;372(6542):642–6.

27. Douangamath A, Fearon D, Gehrtz P, Krojer T, Lukacik P, Owen CD, et al. Crystallographic and electrophilic fragment screening of the SARS-CoV-2 main protease. Nat Commun. 2020;11(1):5047.

28. Pushpakom S, Iorio F, Eyers PA, Escott KJ, Hopper S, Wells A, et al. Drug repurposing: progress, challenges and recommendations. Nat Rev Drug Discov. 2019;18(1):41–58.

29. Wang M, Cao R, Zhang L, Yang X, Liu J, Xu M, et al. Remdesivir and chloroquine effectively inhibit the recently emerged novel coronavirus (2019-nCoV) in vitro. Cell Res. 2020;30(3):269–71.

30. Dong L, Hu S, Gao J. Discovering drugs to treat coronavirus disease 2019 (COVID-19). Drug Discov Ther. 2020;14(1):58–60.

31. Ortega JT, Serrano ML, Pujol FH, Rangel HR. Unrevealing sequence and structural features of novel coronavirus using in silico approaches: The main protease as molecular target. EXCLI J. 2020;19:400–9.

32. Khan MF, Khan MA, Khan ZA, Ahamad T, Ansari WA. Identification of Dietary Molecules as Therapeutic Agents to Combat COVID-19 Using Molecular Docking Studies. Research Square (preprint) 2020.

33. Jurrus E, Engel D, Star K, Monson K, Brandi J, Felberg LE, et al. Improvements to the APBS biomolecular solvation software suite. Protein Sci Publ Protein Soc. 2018;27(1):112–28.

34. MacKerell AD, Bashford D, Bellott M, Dunbrack RL, Evanseck JD, Field MJ, et al. All-Atom Empirical Potential for Molecular Modeling and Dynamics Studies of Proteins. J Phys Chem B. 1998;102(18):3586–616.

35. Li H, Robertson AD, Jensen JH. Very fast empirical prediction and rationalization of protein pKa values. Proteins Struct Funct Bioinforma. 2005;61(4):704–21.

36. O'Boyle NM, Banck M, James CA, Morley C, Vandermeersch T, Hutchison GR. Open Babel: An open chemical toolbox. J Cheminformatics. 2011;3(1):33.

37. Morris GM, Huey R, Lindstrom W, Sanner MF, Belew RK, Goodsell DS, et al. AutoDock4 and AutoDockTools4: Automated docking with selective receptor flexibility. J Comput Chem. 2009;30(16):2785–91.

38. Volkamer A, Kuhn D, Rippmann F, Rarey M. DoGSiteScorer: a web server for automatic binding site prediction, analysis and druggability assessment. Bioinformatics. 2012;28(15):2074–5.

39. Trott O, Olson AJ. AutoDock Vina: Improving the speed and accuracy of docking with a new scoring function, efficient optimization, and multithreading. J Comput Chem. 2010;31(2):455–61.

40. Biovia, D. S. Discovery studio visualizer, 2019. Dassault Systemes, (v19.1.0.15350).

41. Cardoso WB, Mendanha SA. Molecular dynamics simulation of docking structures of SARS-CoV-2 main protease and HIV protease inhibitors. J Mol Struct. 2021;1225:129143.

42. Hakmi M, Bouricha EM, Kandoussi I, Harti JE, Ibrahimi A. Repurposing of known anti-virals as potential inhibitors for SARS-CoV-2 main protease using molecular docking analysis. Bioinformation. 2020;16(4):301–6.

43. Sharma S, Deep S. In-silico drug repurposing for targeting SARS-CoV-2 main protease (Mpro). J Biomol Struct Dyn. 2022;40(7):3003–10.

44. Kumar Y, Singh H, Patel CN. In silico prediction of potential inhibitors for the main protease of SARS-CoV-2 using molecular docking and dynamics simulation based drug-repurposing. J Infect Public Health. 2020;13(9):1210–23.

45. Hammond Jennifer, Leister-Tebbe Heidi, Gardner Annie, Abreu Paula, Bao Weihang, Wisemandle Wayne, et al. Oral Nirmatrelvir for High-Risk, Nonhospitalized Adults with Covid-19. N Engl J Med. 2022;386(15):1397–408.

46. Li J, Lin C, Zhou X, Zhong F, Zeng P, Yang Y, et al. Structural Basis of the Main Proteases of Coronavirus Bound to Drug Candidate PF-07321332. J Virol. 2022;96(8):e02013-21.

47. Owen DR, Allerton CMN, Anderson AS, Aschenbrenner L, Avery M, Berritt S, et al. An oral SARS-CoV-2 Mpro inhibitor clinical candidate for the treatment of COVID-19. Science. 2021;374(6575):1586–93.

48. Liang J, Karagiannis C, Pitsillou E, Darmawan KK, Ng K, Hung A, et al. Site mapping and small molecule blind docking reveal a possible target site on the SARS-CoV-2 main protease dimer interface. Comput Biol Chem. 2020;89:107372.